$$c^2\nabla^2 p(\mathbf{r},t) - \frac{\partial^2 p(\mathbf{r},t)}{\partial t^2} = \frac{\beta c^2}{C_p}\frac{\partial H(\mathbf{r},t)}{\partial t}, \quad (2)$$

where c(m/s) is the speed of sound in the medium, β(K^{-1}) is the isobaric volume expansion coefficient, C_p(J/g K) is the specific heat, and $H(r,t)$ (Jm^{-3}) is the heat energy generated by optical absorption. The solution to Eq. (1) in the time domain can generally be expressed as [1]

$$p(\mathbf{r}',t) = \frac{\beta}{4\pi C_p}\iiint \frac{\mathrm{d}^3\mathbf{r}}{|\mathbf{r}-\mathbf{r}'|}\frac{\partial}{\partial t'}H(\mathbf{r},t')\Big|_{t'=t-|\mathbf{r}-\mathbf{r}'|/c}, \quad (3)$$

where $\mathbf{r}'$ is the observation point. The heat energy $H(\mathbf{r},t)$ can be expressed as the product of the spatial mapping of the absorbed optical energy $A(\mathbf{r})$ and the temporal waveform of the laser pulse $\eta(t)$, allowing Eq. (2) to be rewritten in spherical coordinates as a convolution of the temporal waveform of the laser pulse $\eta(t)$ and a PA waveform excited by a Dirac delta pulse [1,8,24]:

$$p(\mathbf{r}',t) = \frac{\beta}{4\pi C_p}\left(\frac{1}{t}\iint_{|\mathbf{r}-\mathbf{r}'|=ct} A(\mathbf{r}-\mathbf{r}')\mathrm{d}S\right) * \eta'(t), \quad (4)$$

where $\eta'(t)$ is the first time derivative of the temporal profile of the excitation laser pulse. The PA signal $s(\mathbf{r},t)$ detected by an acoustic sensor with an impulse response of $m(t)$ can be expressed as

$$s(\mathbf{r}',t) = \frac{\beta}{4\pi C_p}\left(\frac{1}{t}\iint_{|\mathbf{r}-\mathbf{r}'|=ct} A(\mathbf{r}-\mathbf{r}')\mathrm{d}S\right) * \eta'(t) * m(t). \quad (5)$$

3. Materials and Methods

A. Experimental Setup

We used a reflection mode PA measurement system in which the excitation light irradiation and PA signal detection occur on the same side of the sample, as this detection mode is more appropriate for measuring deep regions of thick biological tissue [22]. A block diagram of this measurement system is shown in Fig. 1. A tunable Ti:sapphire laser (LT-2211, Lotis Tii, Minsk, Belarus) pumped by the second harmonic of a Q-switched Nd:YAG laser (LS-2134, Lotis Tii, Minsk, Belarus) was used to produce excitation light pulses with a width of 20 ns and a repetition frequency of 15 Hz at a wavelength of 720 nm. The excitation pulses were then coupled into a multimode optical fiber with a core diameter of 0.4 mm (M40L02, Thorlabs, Newton, New Jersey).

The optical fiber was arranged coaxially relative to a specially designed ring-shaped acoustic sensor (coaxial PA probe) [22] with inner and outer detection surface diameters of 1.4 and 3.0 mm, respectively. Using a coaxial PA probe made it possible to detect the PA signal along the light transport axis. The

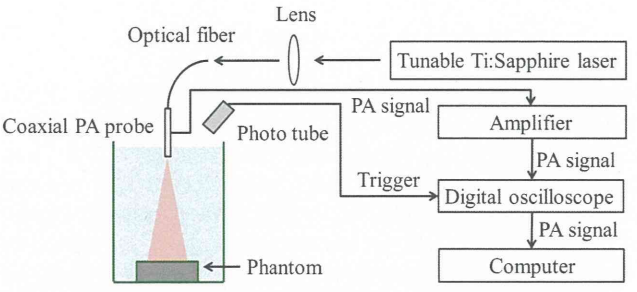

Fig. 1. Experimental setup for reflection mode measurement of PA signals.

acoustic sensor was fabricated from a 50-μm-thick piezoelectric film P(VDF-TrFE) (KF piezo-film, Kureha Corp., Tokyo, Japan), which has a wider frequency bandwidth than that of a lead zirconium titanate piezoelectric ceramic [22]. The acoustic sensor was already calibrated within the frequency range of 1–20 MHz by a secondary calibration method [25] using a precalibrated hydrophone (HPM05/3, Precision Acoustics, Dochester, UK). The frequency of maximum sensitivity was 1.7 MHz, and the 6 dB frequency band was 1.2–14.4 MHz. Using an acoustic sensor with such a wide frequency bandwidth enabled us to analyze the spectra of the PA signals over a wide frequency range. The PA signals detected by the acoustic sensor were amplified by a low-noise field-effect transistor amplifier (SA-220F5, NF Electronic Instruments, Yokohama, Japan) and then recorded by a digital oscilloscope (DSO8104A, Agilent Technology, Santa Clara, California) with a sampling rate of 2 GSa/s.

B. Computational Simulation

To calculate the relationship between the frequency spectra of the PA signals and the effective attenuation coefficients of optical absorbers, we used Eq. (4) as the basis for an analytical simulation of the generation of PA pressure waves and the detection of PA signals. In the model, PA pressure waves were generated by irradiating planar optical absorbers with excitation light pulses (pulsewidth = 20 ns) via an optical fiber. The resulting PA signals were detected by a ring-shaped acoustic sensor with inner and outer detection surface diameters of 1.4 and 3.0 mm, respectively. The acoustic sensor and optical fiber were coaxially combined and placed at a distance of 45 mm from the optical absorber.

Because optical scattering in the optical absorber was neglected for the purposes of this simulation, the effective attenuation coefficients, μ_{eff}, were proportional to the optical absorption coefficients μ_a. Thus, the amount of optical energy $A(r,\theta,\varphi)$ absorbed by an optical absorber with an absorption coefficient of μ_a could be formulated using spherical coordinates as

$$A(r,\theta,\phi) = \frac{r\sin\theta}{r_0\sin\theta_0}F(r_0\cos\theta\cos\phi, r_0\cos\theta\sin\phi) \times \exp\left(-\int_0^r \mu_a(r',\theta,\phi)\mathrm{d}r'\right), \quad (6)$$

$$\mu_a(r,\theta,\phi) = \mu_a \quad \text{where } r\cos\theta < z_0, \tag{7}$$

where F is the fluence of the excitation light pulses measured by a beam profiler (SP620, Ophir, Israel), which is placed on the surface 17.5 mm from the output end of the optical fiber. The optical absorption coefficients μ_a were varied over a range of 10–40 cm^{-1}, which corresponds to the effective attenuation coefficients of blood over a wavelength range of 700–900 nm with a hematocrit concentration of 40%–50% and an oxygen saturation of 0%–100% [3].

Because the time increment of this simulation was 3 ns, the Nyquist frequency was 166 MHz, which is sufficiently higher than the frequencies of the PA signals. The size and shape of the detection surface were taken into account by performing a surface integration process in which the detection surface was discretized into small elements and the PA signals detected by each element were calculated using Eq. (4). Finally, the individual signals were numerically integrated in order to calculate the total PA signal detected by the sensor surface.

The impulse response function of the acoustic sensor was measured, and then incorporated into the simulated PA signals. The impulse response function $m(t)$ was obtained by measuring a PA signal produced at a spatial point [8,26]. The PA signal was produced by irradiating an excitation pulse focused by a convex lens with focal length of 200 mm onto carbon suspension with an optical absorption coefficient of 2000 cm^{-1}. Because the excitation pulse was absorbed within a volume smaller than the ultrasound wavelength, the optical absorption distribution $A(\mathbf{r}-\mathbf{r}')$ in Eq. (4) can be approximated by Dirac's delta function $\delta(\mathbf{r}-\mathbf{r}')$. Thus, the PA signal can be expressed as follows using Eq. (5):

$$s_\delta(\mathbf{r}',t) = \frac{\beta}{4\pi C_p}\frac{1}{|\mathbf{r}-\mathbf{r}'|}\eta'\left(t-\frac{|\mathbf{r}-\mathbf{r}'|}{c}\right) * m(t). \tag{8}$$

Thus, by substituting the following equation into Eq. (5), the impulse response function of the acoustic sensor was incorporated into the simulation:

$$m(t) * \eta'(t) = \frac{4\pi C_p}{\beta}|\mathbf{r}-\mathbf{r}'|s_\delta\left(\mathbf{r}',t+\frac{|\mathbf{r}-\mathbf{r}'|}{c}\right). \tag{9}$$

C. Experiment Using Phantoms

To verify the relationship between the frequency spectra of the PA signals and the effective attenuation coefficients of optical absorbers, we measured the PA signals produced by phantoms having various optical absorption coefficients. Because of its resistance to photobleaching, a specific black ink (Black Ink, Pilot, Tokyo, Japan) was used as an optical absorber. The ink was diluted with water down to six different concentrations. The diluted black inks were then placed in a cylindrical container with a diameter of 35 mm and a thickness of 9 mm, and the top surface of the container was sealed with an 11-μm-thick clear polymer film selected to ensure minimal attenuation of excitation light pulses and PA signals. The coaxial PA probe was placed perpendicular to the top surface of the phantom at a distance of 45 mm, and then both the phantom and the probe were immersed in degassed water. The experiment was performed with excitation pulse energies of 300, 600, and 1200 μJ.

The optical attenuation coefficients of the diluted inks quantified from the PA signals were compared with the optical attenuation coefficients measured using a spectrophotometer (U-3300, Hitachi High-technologies, Tokyo, Japan)

D. Frequency Analysis of PA Signals

The CWT is a spectral analysis method that can produce time-resolved frequency spectra of PA signals. This method differs from the FT, which produces a frequency spectrum without time resolution. The CWT modulus of a signal $T(a,b)$ is defined as the convolution of the temporal signal $p(t)$ and the dilated and temporally translated version of the wavelet function $\Psi(t)$ [14,17,27–30]:

$$T(a,b) = a^{-\frac{1}{2}}\int_{-\infty}^{\infty} p(t)\Psi^*\left(\frac{t-b}{a}\right)dt, \tag{10}$$

where $\Psi^*(t)$ is the complex conjugate of $\Psi(t)$, a is the dilation parameter, and b is the location parameter. Here, the complex Morlet wavelet, which is defined as a complex sinusoid with a Gaussian envelope [15,28,30], is used:

$$\Psi(t) = \pi^{-\frac{1}{4}}(e^{-i\omega_0 t} - e^{-\omega_0^2 t})e^{-\frac{t^2}{2}}, \tag{11}$$

where ω_0 is the central frequency of the wavelet, which determines the number of sinusoidal waves within the Gaussian envelope. The dilation parameter a can be transformed into the frequency f using the equation $f = \omega_0/a$, where the time t replaces the location parameter b. Thus, the CWT produces time-resolved frequency spectra $T(f,t) = T(\omega_0/a, b)$ with a power given by $|T(f,t)|^2 = \mathrm{Re}[T(f,t)]^2 + \mathrm{Im}[T(f,t)]^2$.

The time-resolved spectra were compared with the power spectra of the PA signal, which were calculated using the FT. The FT was applied to the PA signals cropped with a rectangular window with a time width of 4 μs. This time width was wider than the recording length. A frequency resolution of 10 kHz was achieved by padding the PA signal with zeros.

4. Results

A. Computational Simulation

PA signals produced by optical absorbers with effective attenuation coefficients of between 10 and 40 cm^{-1} were calculated; Fig. 2 shows the temporal

waveforms of the signals produced by the absorbers with coefficients of 17 and that of 30 cm^{-1}. Although the leading edges of the PA signals shown in the figure have nearly identical slopes, their trailing edges differ; this suggests that only the trailing edges of PA signals depend on the effective attenuation coefficients of the optical absorbers. The time-resolved frequency spectrum of the PA signal produced by the optical absorber with an effective attenuation coefficient of 17 cm^{-1} is displayed in Fig. 3(a), which shows the peaks of the PA signal temporal waveforms observed at time $t = 0$. The local maxima originating from both positive and negative parts of the temporal waveform were observed at t_1 and t_2, respectively.

The profiles of the time-resolved frequency spectrum at times t_1 and t_2 are displayed in Fig. 3(b). The dominant frequencies were determined by calculating the frequencies satisfying $d|T(f,t)|^2/df = 0$ and are shown in Fig. 4 as functions of time. The dominant frequencies in the figure all have maximum values at time $t = -0.015$ μs, which coincides nearly perfectly with the peak time of the temporal waveform; it is therefore apparent that the maximum values of the dominant frequencies depend on both the leading and trailing edges of the PA signals. Because the slopes of the trailing edges of the signals depend on the effective attenuation coefficients of the optical absorbers, we can use the maximum values of the dominant frequencies to quantify these coefficients.

The maximum values of the dominant frequencies and the peak frequencies of the power spectra are shown in Fig. 5 as functions of the effective attenuation coefficients of the optical absorbers. The peak frequencies of the power spectra are shown in Fig. 5. Owing to the variation in the acoustic sensor sensitivity at frequencies of less than 1 MHz, the peak frequency of the power spectra varied nonlinearly with the effective attenuation coefficients of the

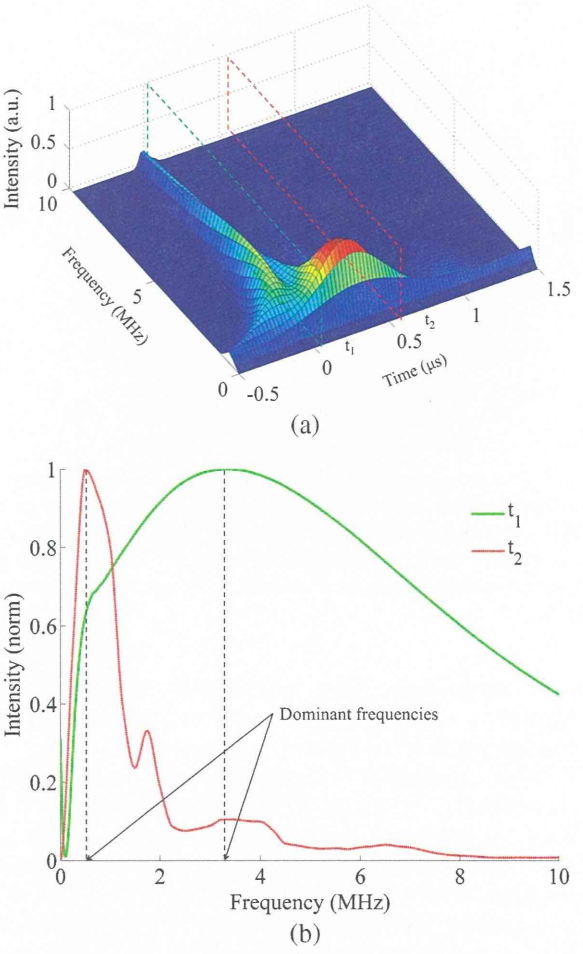

Fig. 3. Analysis of calculated PA signals produced by an optical absorber with an effective attenuation coefficient of 17 cm^{-1}. (a) Time-resolved frequency spectra of PA signal calculated using CWT. The maxima originating from the positive and negative parts of the PA signal were observed at times t_1 and t_2, respectively. (b) Profiles of time-resolved frequency spectra with respect to times t_1 and t_2

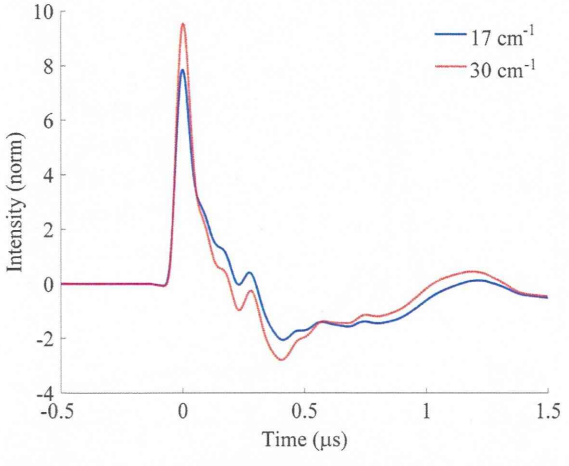

Fig. 2. Temporal waveforms calculated for PA signals produced by optical absorbers with effective attenuation coefficients of 17 cm^{-1} (blue) and 30 cm^{-1} (red), respectively. The amplitudes of the PA signals are normalized.

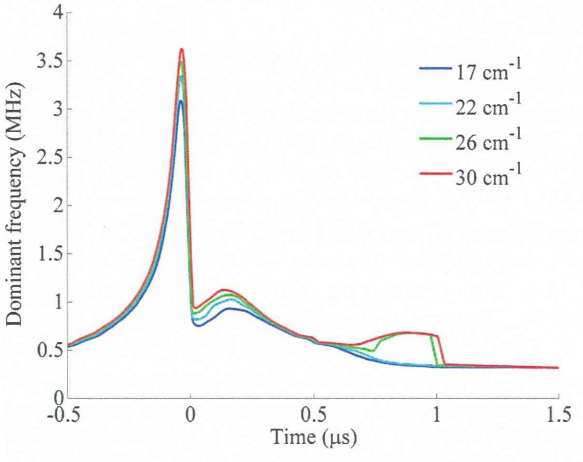

Fig. 4. Dominant frequency of the PA signal produced from optical absorbers with various effective attenuation coefficient as a function of time.

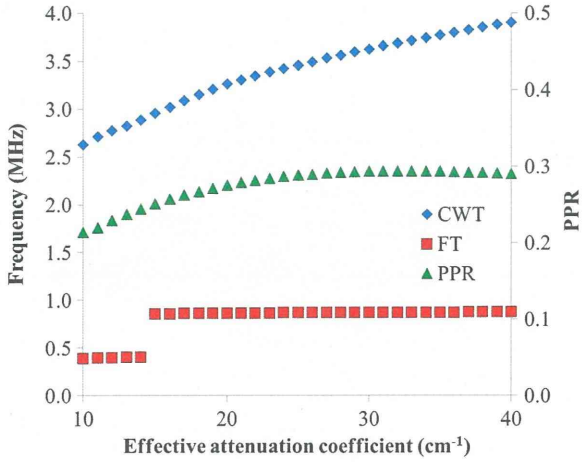

Fig. 5. Relationship between the maximum values of dominant frequencies of calculated PA signals and the effective attenuation coefficients of optical absorbers (blue, diamond). The peak frequencies of power spectra calculated by using FT (red, square) and PPR calculated from temporal waveform (green, triangle) are also plotted.

optical absorbers. The maximum values of the dominant frequencies, in contrast, monotonically increased as the coefficient increased.

We also calculated the peak-to-peak ratio (PPR) of the temporal waveform, which is defined as the ratio of the positive peak and negative peaks. Wang and Wang proposed to use this parameter to determine the optical absorption coefficient [8]. The peaks of the dominant frequencies and the PPRs are shown in Fig. 4 as functions of the effective attenuation coefficients of the optical absorbers. Both parameters increased as the coefficient increased. However, the PPR became constant for an effective attenuation coefficient larger than 30 cm^{-1}.

B. Experiment

PA signals produced by phantoms consisting of diluted black inks with six concentrations were measured using a coaxial PA probe. The effective attenuation coefficients of the diluted inks measured using a spectrophotometer were 13, 17, 22, 26, 30, and 35 cm^{-1}.

The time-resolved frequency spectrum of the PA signal produced by the optical absorber with an effective attenuation coefficient of 13 cm^{-1} is displayed in Fig. 6(a), which shows the peaks of the PA signal temporal waveforms observed at time $t = 0$. The profiles of the time-resolved frequency spectrum at times t_1 and t_2 are displayed in Fig. 6(b). The dominant frequencies are shown in Fig. 7 as functions of time. The dominant frequencies calculated from the CWT, the peak frequencies calculated from the FT of the PA signals, and the PPR are displayed in Fig. 8. Both the dominant frequency and the PPRs of the measured PA signals coincided with those of the simulated PA signals. The peak frequencies of the PA signals calculated using the FT exhibited no correlation with the effective attenuation coefficients of the optical absorbers.

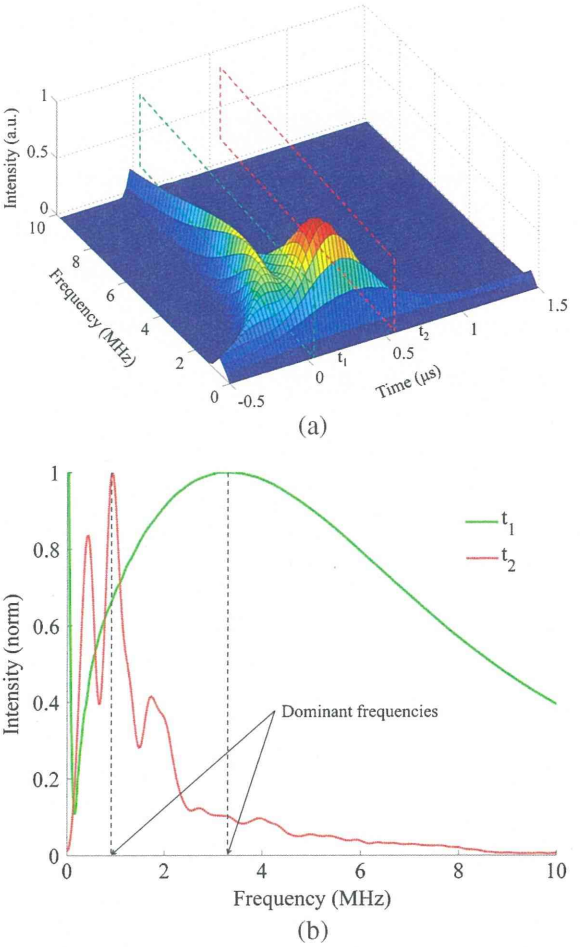

Fig. 6. Analysis of experimentally measured PA signals produced by an optical absorber with an effective attenuation coefficient of 17 cm^{-1}. (a) Time-resolved frequency spectra of PA signal calculated using CWT. The maxima originating from the positive and negative parts of the PA signal were observed at times t_1 and t_2, respectively. (b) Profiles of time-resolved frequency spectra with respect to times t_1 and t_2.

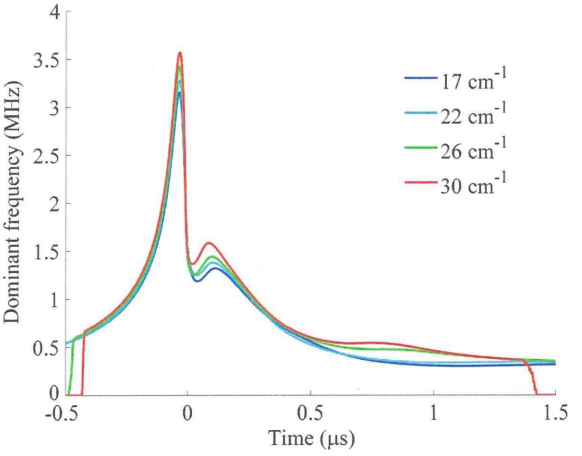

Fig. 7. Dominant frequency of the PA signal produced from optical absorbers with various optical absorption coefficients as a function of time.

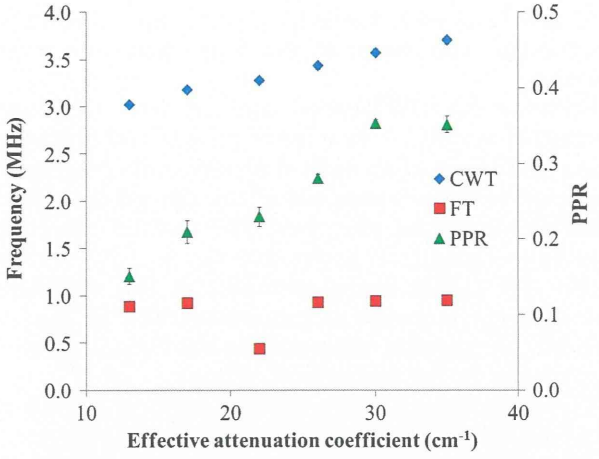

Fig. 8. Relationship between the maximum values of the dominant frequencies of the experimentally measured PA signals and the effective attenuation coefficients of optical absorbers (blue, triangle). The peak frequencies of power spectra calculated using FT (red, square) and PPR calculated from temporal waveform (green, triangle) are also plotted (error bar: standard deviation, $n = 4$).

The effective attenuation coefficients were determined using both the PPRs and the maximum value of the dominant frequencies. The relationship between both parameters and the effective attenuation coefficients obtained from the simulation was used to quantify the optical attenuation coefficient obtained experimentally from both parameters. Figure 9 compares the effective attenuation coefficients quantified using the CWT and spectrophotometer measurement. The linearity of the curve indicates agreement between two measurement methods. The mean square error of the spectrophotometer measurements was 2.0 cm^{-1}, whereas the uncertainties of the measurements calculated from the standard deviations of the maximum values of the dominant frequencies were less than 1.3 cm^{-1}. The effective attenuation

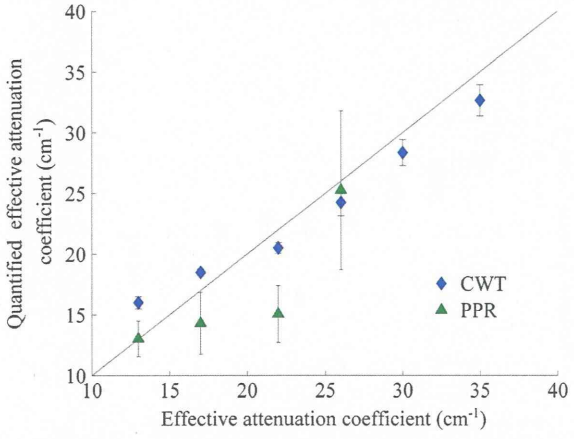

Fig. 9. Effective attenuation coefficients of the optical absorbers calculated from experimentally measured PA signals using CWT (blue, diamond) and temporal waveform (green, triangle) as a function of measured by spectrophotometer. The ideal fit line is also plotted (black, dotted) (error bar: standard deviation, $n = 4$).

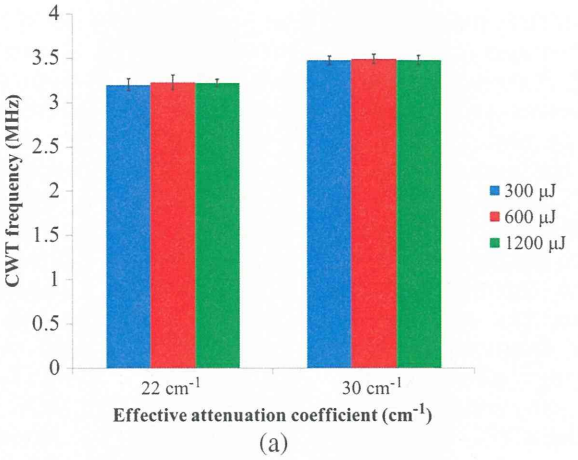

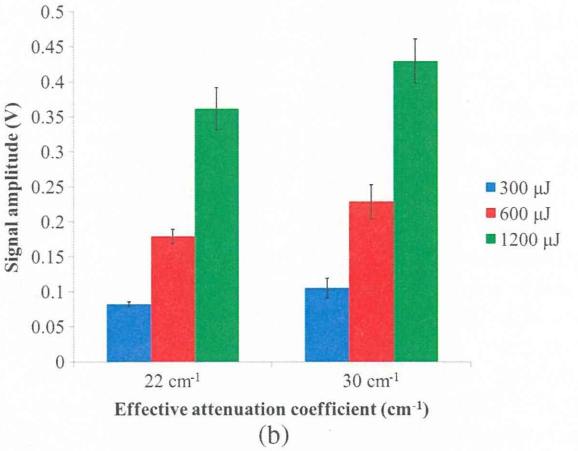

Fig. 10. (a) Maximum values of the dominant frequencies and (b) amplitude of PA signals produced from optical absorbers with effective attenuation coefficients of 22 and 30 cm^{-1}. The pulse energy of the excitation pulse was 300, 600, and 1200 μJ.

coefficients calculated from the PPRs are also shown in Fig. 9. Because the relationship between the PPR and the effective attenuation coefficient displayed in Fig. 5 was constant for coefficients larger than 30 cm^{-1}, we excluded these data points. The mean square error of the coefficients calculated from the PPRs was 3.7 cm^{-1}.

The maximum values of the dominant frequencies and the amplitudes of PA signals measured at various excitation pulse energies are shown in Figs. 10(a) and 10(b), respectively. Although the amplitude of the PA signal was proportional to the excitation pulse energy, the maximum value of the dominant frequency was constant for various excitation energies.

5. Discussion

This study shows that the maximum values of the dominant frequencies of PA signals obtained by CWT accurately represent the effective attenuation coefficients of optical absorbers.

The experimental and simulation results of this study suggest that the temporal resolution of the CWT makes the quantification method more robust

than that using the FT. The peak frequencies of the power spectra of the measured PA signals shown in Fig. 8 deviate from a linear relationship with the effective attenuation coefficients at the coefficients of 13 and 17 cm^{-1}. These deviations were caused by the variation in the acoustic sensor sensitivity at frequencies of less than 1 MHz. Since the FT calculates the frequency spectra without time resolution, the negative part of the PA signals that has long time duration dominates the frequency spectra. Since the negative part of PA signals consists of low frequency content, the peak frequency was strongly affected by the variation in the acoustic sensor sensitivity at frequencies of less than 1 MHz. In using CWT, the maximum values of the dominant frequencies will be less affected by the variation in the acoustic sensor sensitivity at frequencies of less than 1 MHz. This is because CWT divided the frequency contents of the positive and negative parts of the PA signals, and the frequency content of the positive part was selectively extracted.

The simulation and experimental results of this study also suggest that the CWT exhibits greater robustness than the PPR to distortions of the waveforms due to the detector impulse response functions. Another group proposed using the PPR calculated from the temporal waveform for quantification of the optical absorption coefficient using a forward-mode PA measurement system. In this study, we adopted this method for the reflection mode PA measurement system. In the reflection mode system, the negative peak of the PA signal was strongly affected by distortion due to the impulse response of the acoustic sensor, because it overlapped the residual oscillation of strong positive peak. Because the intensity of the negative peak was dominated by the residual oscillation of the positive peak, the PPR became constant for an effective attenuation coefficient larger than 30 cm^{-1} in the simulated result shown in Fig. 5.

We quantified the effective attenuation coefficient of a phantom made of diluted black ink by comparing the maximum values of the dominant frequencies calculated from the measured PA signal and from simulated PA signals. As shown in Fig. 9, we were able to calculate this value to within an error of 2.0 cm^{-1}. The calculated accuracy of the blood oxygen saturation depends on the difference in the effective attenuation coefficient between oxygenated and deoxygenated blood. This difference is known to be wavelength dependent, with a peak at 756 nm; by using excitation light at this wavelength, therefore, the blood oxygen saturation can be calculated accurately. At a wavelength of 756 nm, the effective attenuation coefficients of blood with oxygen saturation levels of 2.3% and 99.6% are 27.5 and 20.0 cm^{-1}, respectively, [3]. As the effective attenuation coefficient of the data set used to determine these values varies at a rate of -0.077 $cm^{-1}/\%$, a 2.0 cm^{-1} mean square error in the effective attenuation coefficient corresponds to a 24% error in the oxygen saturation. This error can be reduced by measuring the effective attenuation coefficient at multiple excitation wavelengths.

Because the CWT-based method uses frequency instead of amplitude to quantify the effective attenuation coefficient of an optical absorber, its results are expected to be independent of the optical fluence on the surface of the absorber. The results shown in Fig. 9 experimentally prove that the maximum value of the PA signal is independent of the excitation pulse energy; thus the parameter enables quantification of the effective attenuation coefficient without compensating for the optical fluence.

The challenges of the proposed method are the effects of the excitation beam profile and optical absorber shape on the dominant frequency of the PA signals. The dependence of the maximum value of the dominant frequency on the beam profile and the beam diameter on the optical absorber surface is shown in Fig. 11. The impulse response of the acoustic sensor was not incorporated into this simulation. The maximum values of the dominant frequency decrease as the beam diameter expands. The dominant frequency of the PA signals depends on both the leading and trailing edges of their temporal waveforms of PA signals. These waveforms of PA signals are determined by the spatial distribution of the optical energy absorption within the sensitive volume of an acoustic sensor. Because we used the unfocused acoustic sensor with a large sensitive volume, the spatial distribution of the optical energy determined by both the diameter and shape of the excitation beam directly affects the dominant frequency.

If the sensitive volume of the acoustic sensor is smaller than the spatial distribution of the optical absorption, the temporal waveforms of the PA signals are less sensitive to the beam diameter. Thus, focused acoustic sensors with a focused sensitive volume can be used to reduce the effects of both the profile and the diameter of the excitation beam.

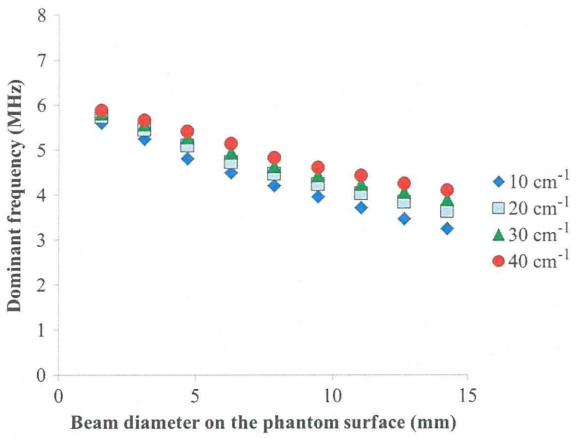

Fig. 11. Maximum value of the dominant frequency of simulated PA signals using ideal acoustic sensor as a function of the beam diameter on the surface of the optical absorber.

The use of focused acoustic sensors also reduces the effect of the optical absorber shape. If the optical absorber is sufficiently larger than the sensitive volume of the acoustic sensor, the surface of the optical absorber can be treated as a flat surface [9,13].

In this study, the proposed method was tested using the simplest model: a planar phantom placed in nonscattering media. If optical scattering is present, the proposed method suffers from two problems. One is the expansion of the spatial distribution of excitation light due to optical scattering. Because this problem is similar to the effect of the diameter and profile of the excitation beam, it is possible to reduce it by using a focused acoustic sensor. We are currently fabricating a ring-shaped focused acoustic sensor with a concave detection surface. The other problem is the change of the optical penetration depth due to the optical scattering. To address this problem, it is necessary to calculate the optical penetration depth considering the optical scattering. In some cases, the effective attenuation coefficient calculated using Eq. (1) would be effective.

6. Conclusions

In this paper, we proposed a CWT-based method for quantifying the effective attenuation coefficients of optical absorbers using PA signals. Because this method uses the frequency instead of the amplitude to characterize the attenuation coefficient, it is unaffected by the fluence on the surface of the optical absorber. The CWT was used to calculate the time-resolved frequency spectra of PA signals, from which the maximum values of the dominant frequencies were calculated in turn. We demonstrated that the maximum values of the dominant frequencies of PA signals are linearly correlated with the effective attenuation coefficients of optical absorbers and, on the basis of this finding, the coefficients of the optical absorbers can be calculated to with mean square error of 2.0 cm^{-1}, which is much smaller than the errors obtained in calculating the quantified PPR.

We demonstrated that the CWT has advantages over the FT in terms of time resolution. The improved time resolution of CWT enables the separation of the PA signal from the residual oscillation in the time domain. The challenges of the proposed method are the effects of the excitation beam profile and optical absorber shape; to reduce such geometrical effects, we are fabricating a ring-shaped focused acoustic sensor with a concave detection surface.

This research was partially supported by a Health and Labor Science Research Grant for Research on Medical Device Development, JST Collaborative Research based on Industrial Demand (*In vivo* Molecular Imaging: toward Biophotonics Innovations in Medicine), and JSPS KAKENHI Grant No. 25750192. The authors appreciate the contributions of Mr. Y. Ikeda, Mr. H. Ishihara, Ms. M. Tanikawa, and Ms. Y. Mayumi to this study. Experiments were supported by the Laboratory Center, National Defense Medical College.

References

1. M. Xu and L. V. Wang, "Photoacoustic imaging in biomedicine," Rev. Sci. Instrum. **77**, 041101 (2006).
2. S. L. Jacques and S. A. Prahl, "Absorption spectra for biological tissues (Oregon Medical Laser Center, OR)" (2004), retrieved March 12, 2013, http://omlc.ogi.edu/spectra/.
3. J. Laufer, C. Elwell, D. Delpy, and P. Beard, "In vitro measurements of absolute blood oxygen saturation using pulsed near-infrared photoacoustic spectroscopy: accuracy and resolution," Phys. Med. Biol. **50**, 4409–4428 (2005).
4. A. Roggan, M. Friebel, K. Dorschel, A. Hahn, and G. Muller, "Optical properties of circulating human blood in the wavelength range 400–2500 nm," J. Biomed. Opt. **4**, 36–46 (1999).
5. M. Sivaramakrishnan, K. Maslov, H. F. Zhang, G. Stoica, and L. V. Wang, "Limitations of quantitative photoacoustic measurements of blood oxygenation in small vessels," Phys. Med. Biol. **52**, 1349–1361 (2007).
6. R. O. Esenaliev, I. V. Larina, K. V. Larin, D. J. Deyo, M. Motamedi, and D. S. Prough, "Optoacoustic technique for noninvasive monitoring of blood oxygenation: a feasibility study," Appl. Opt. **41**, 4722–4731 (2002).
7. B. Cox, J. G. Laufer, S. R. Arridge, and P. C. Beard, "Quantitative spectroscopic photoacoustic imaging: a review," J. Biomed. Opt. **17**, 061202 (2012).
8. Y. Wang and R. Wang, "Photoacoustic recovery of an absolute optical absorption coefficient with an exact solution of a wave equation," Phys. Med. Biol. **53**, 6167–6177 (2008).
9. Z. Guo, C. Favazza, A. Garcia-Uribe, and L. V. Wang, "Quantitative photoacoustic microscopy of optical absorption coefficients from acoustic spectra in the optical diffusive regime," J. Biomed. Opt. **17**, 066011 (2012).
10. J. Laufer, B. Cox, E. Zhang, and P. Beard, "Quantitative determination of chromophore concentrations from 2D photoacoustic images using a nonlinear model-based inversion scheme," Appl. Opt. **49**, 1219–1233 (2010).
11. J. A. Viator, S. L. Jacques, and S. A. Prahl, "Depth profiling of absorbing soft materials using photoacoustic methods," IEEE J. Sel. Top. Quantum Electron. **5**, 989–996 (1999).
12. M. Jaeger, M. Hejazi, and M. Frenz, "Diffraction-free acoustic detection for optoacoustic depth profiling of tissue using an optically transparent polyvinylidene fluoride pressure transducer operated in backward and forward mode," J. Biomed. Opt **10**, 024035 (2005).
13. Z. Guo, S. Hu, and L. V. Wang, "Calibration-free absolute quantification of optical absorption coefficients using acoustic spectra in 3D photoacoustic microscopy of biological tissue," Opt. Lett. **35**, 2067–2069 (2010).
14. T. Hirasawa, M. Ishihara, K. Tsujita, K. Hirota, K. Irisawa, M. Kitagaki, M. Fujita, and M. Kikuchi, "Continuous wavelet-transform analysis of photoacoustic signal waveform to determine optical absorption coefficient," Proc. SPIE **8223**, 822333 (2012).
15. T. Hirasawa, M. Fujita, S. Okawa, T. Kushibiki, and M. Ishihara, "Improvement in quantifying optical absorption coefficients based on continuous wavelet-transform by correcting distortions in temporal photoacoustic waveforms," Proc. SPIE **8581**, 85814J (2013).
16. S. H. Holan and J. A. Viator, "Automated wavelet denoising of photoacoustic signals for circulating melanoma cell detection and burn image reconstruction," Phys. Med. Biol. **53**, N227–N236 (2008).
17. J. A. Viator, B. Choi, M. Ambrose, J. Spanier, and J. S. Nelson, "In vivo port-wine stain depth determination with a photoacoustic probe," Appl. Opt. **42**, 3215–3224 (2003).
18. T. Lu, J. Jiang, Y. Su, Z. Song, J. Yao, and R. K. Wang, "Signal processing using wavelet transform in photoacoustic tomography," Proc. SPIE **6439**, 64390L (2007).
19. Z. Li, H. Li, Z. Zeng, W. Xie, and W. R. Chen, "Determination of optical absorption coefficient with focusing photoacoustic imaging," J. Biomed. Opt **17**, 061216 (2012).

20. Z. Li, H. Li, H. Chen, and W. Xie, "In vivo determination of acute myocardial ischemia based on photoacoustic imaging with a focused transducer," J. Biomed. Opt **16**, 076011 (2011).
21. S. A. Ermilov, R. Gharieb, A. Conjusteau, T. Miller, K. Mehta, and A. A. Oraevsky, "Data processing and quasi-3D optoacoustic imaging of tumors in the breast using a linear arc-shaped array of ultrasonic transducers," Proc. SPIE **6856**, 685603 (2008).
22. M. Ishihara, M. Sato, N. Kaneshiro, G. Mitani, S. Sato, J. Mochida, and M. Kikuchi, "Development of a diagnostic system for osteoarthritis using a photoacoustic measurement method," Lasers Surg. Med. **38**, 249–255 (2006).
23. C. Li and L. V. Wang, "Photoacoustic tomography and sensing in biomedicine," Phys. Med. Biol. **54**, R59–R97 (2009).
24. K. Irisawa, T. Hirasawa, K. Hirota, K. Tsujita, and M. Ishihara, "Influence of laser pulse width to the photoacoustic temporal waveform and the image resolution with a solid state excitation laser," Proc. SPIE **8223**, 82232W (2012).
25. V. Wilkens and C. Koch, "Amplitude and phase calibration of hydrophones up to 70 MHz using broadband pulse excitation and an optical reference hydrophone," J. Acoust. Soc. Am. **115**, 2892–2903 (2004).
26. A. Rosenthal, V. Ntziachristos, and D. Razansky, "Optoacoustic methods for frequency calibration of ultrasonic sensors," IEEE Trans. Ultrason. Ferroelectr. Freq. Control **58**, 316–326 (2011).
27. C. Torrence and G. P. Compo, "A practical guide to wavelet analysis," Bull. Am. Meteorol. Soc. **79**, 61–78 (1998).
28. P. Addison, J. Watson, and T. Feng, "Low-oscillation complex wavelets," J. Sound Vib. **254**, 733–762 (2002).
29. T. Kijewski and A. Kareem, "Wavelet transforms for system identification in civil engineering," Comput.-Aided Civil Infrastruct. Eng. **18**, 339–355 (2003).
30. P. S. Addison, *The Illustrated Wavelet Transform Handbook*, Introductory Theory and Applications in Science, Engineering, Medicine and Finance (IOP, 2005).

Reconstruction of the optical properties of inhomogeneous medium from photoacoustic signal with l_p sparsity regularization

Shinpei Okawa, Takeshi Hirasawa, Toshihiro Kushibiki and Miya Ishihara

Department of Medical Engineering, National Defense Medical College, 3-2 Namiki, Tokorozawa, Saitama, 359-8513, Japan

ABSTRACT

A method to reconstruct the optical properties in the inhomogeneous medium from the photoacoustic (PA) signal is discussed. The forward modeling of the propagations of the excitation light and of the photoacoustic pressure is carried out with the finite element method. The inverse problem is formulated with a linear equation relating the optical properties and time-domain PA signals. By solving the inverse problem, the distribution of the optical properties in the optically inhomogeneous medium is reconstructed. The measurement noise and the mismatches between the actual measurement conditions and the forward model cause artifacts in the reconstructed image. To reduce the artifacts and to obtain high resolved reconstructed image, we uses the l_p sparsity regularization method which minimizes the l_p norm of the solution of the inverse problem. It is demonstrated by some numerical simulations that the regularization method using the l_p norm obtains a sparse distribution of the changes in the optical properties. The images reconstructed with the l_p sparsity regularization are compared those with truncated singular value decomposition.

Keywords: photoacoustic imaging, optical property, regularization, truncated singular value decomposition, inverse problem

1. INTRODUCTION

Photoacoustic (PA) imaging[1] have garnered a lot of attentions in recent years. In PA imaging, nano-second pulse laser illuminates biological tissues, and then the energy of the light absorbed by the choromophores in tissues is converted into heat. As a result, elastic wave caused by the thermal expansion of the tissues is emitted. The detected elastict wave, PA signal namely, can be used to image of the distribution of the chromophores.

Although, because of the limited penetration depth of the excitation light, PA technique can image shallower regions than the other imaging modalities such as X-ray CT and MRI can, the spatial resolution of PA imaging is much higher than that of the other modalities. The chromophores, which are the sources of the PA signal, can be located more easily than optical tomography detecting light which is strongly attenuated by scattering and absorption by the tissues. The high resolution feature and the principle exploiting the absorption of the light allow us to obtain precise microvasular images.

PA image is obtained via reconstruction process. Delay-and-sum backprojection and circular backprojection originally developed for ultrasound imaging can readily be implemented. Xu et al presented some methods, such as frequency-domain reconstruction and universal backprojection which are analytically derived from PA wave equation.[2] For the acoustically homogeneous medium, those analytical reconstruction method works well. k-space method is efficient for the forward calculation of PA propagation in frequency domain. By employing k-space pseudospectral methods, Treeby et al reconstructed high-quality image of the vasculature by using time-reversal method and compensating the acoustic absorption in acoustically heterogeneous medium.[3]

By taking account of the excitation light propagation, the optical properties and concentrations of the chromophores in optically inhomogeneous medium can be estimated. Laufer et al achieved model-based inversion scheme reconstructing the chromophore concentration. This method minimizes the error between the measured and predicted images by using the forward model with photon diffusion equation (PDE) for light propagation

Shinpei Okawa: E-mail: okawa@ndmc.ac.jp, Telephone: +81 4 2995 1596

Photons Plus Ultrasound: Imaging and Sensing 2013, edited by Alexander A. Oraevsky, Lihong V. Wang,
Proc. of SPIE Vol. 8581, 858135 · © 2013 SPIE · CCC code: 1605-7422/13/$18 · doi: 10.1117/12.2003656

and k-space method for PA pressure propagation.[4] Yuan et al reconstructs the optical absorption coefficient using PDE and finite element method (FEM) based PA image reconstruction algorithm.[5]

The reconstructed image is always aggravated by noise and insufficient forward modeling due to the nature of inverse problems. The mismatches between the actual measurement conditions and the forward model cause artifacts and low spatial resolution image. A simple forward model, however, is preferable in the sense of the computational cost for practical use.

In this paper, we attempted to improve the quality of the image of the optical properties reconstructed from PA signals by employing the l_p sparsity regularization method which minimizes the l_p norm of the solution and obtains sparse solution.[6] The PA forward model is constructed by PA wave equation, and the propagation of the light in optically inhomogeneous medium is taken into account by using PDE. Then the relation between the detected PA signal and the optical properties in the medium is formulated as a linear equation by using FEM. The image is reconstructed by minimizing the error between the detected and calculated PA signals. The l_p norm of the absorption coefficient is minimized simultaneously. Some numerical simulations were carried out to verify the effect of the l_p sparsity regularization and compared the performance of the l_p sparsity regularization to that of truncated singular value decomposition (TSVD) method.

2. FORWARD MODELING

2.1 PA pressure propagation

The nano-second pulse light illuminating the biological medium is propagated and absorbed by the chromophores in tissues. The absorption takes place on a femtosecond timescale. And the absorbed light energy is converted into the heat, which causes the PA pressure, on a sub-nanosecond timescale. When the pulse width of the excitation light is so small that thermal diffusion can be neglected, the propagation of the PA pressure in an acoustically homogeneous medium is described by the following PA wave equation,[7]

$$\left\{-\nabla^2 + \frac{1}{v^2}\frac{\partial^2}{\partial t^2}\right\} p(r,t) = \hat{\Gamma}\frac{\partial}{\partial t}H, \tag{1}$$

where v is the speed of the PA pressure, p, the PA pressure, $\hat{\Gamma}$, Grüneisen parameter associated with the PA efficiency, and H, absorbed energy density. The PA source term is the energy of the light absorbed by tissues, which can be calculated by solving following photon diffusion equation. FEM was employed to solve this forward problem in this study.

2.2 Light propagation

The source of the PA signal depends on the fluence rate of the excitation light and the absorption coefficient.The chromophores absorbing the light generate PA pressure. The absorbed energy density is given by $H = \mu_a\Phi$ with the absorption coefficient μ_a and the fluece rate Φ, which are calculated with PDE.

The light is scattered and absorbed by biological tissues. The propagation of the excitation light is described by the radiative transfer equation (RTE).[8] In this paper, we used following time-independent PDE which is the approximation of RTE,

$$\{-\nabla \cdot D(r)\nabla + \mu_a(r)\}\,\Phi(r) = q_0(r), \tag{2}$$

where $D = 1/(3\mu_s')$ is the diffusion coefficient with the scattering coefficient μ_s', μ_a, the absorption coefficient, Φ, the fluence rate of light, q_0, the light source, and r, the position. PDE is hold when the medium is thick enough and the time after the pulse light incidence is longer. The boundary condition is given as $-n \cdot D\nabla\Phi = 1/(2A)\Phi$ where n is the vector normal to the surface of the medium, and A is the parameter depending on the internal reflection ratio. PDE can be solved by using FEM.